AN EXPERIMENTAL STUDY ON VERTICAL LOAD RESISTANCE OF CFT COLUMN-FLAT PLATE JOINTS

T. YAMAGUCHI [1], K. SHIMAZAKI [2] and H. SATOU [3]

[1] *Ando corporation, Tokyo, Japan*
[2] *Professor, Dept. of Architecture and Building Engineering, Kanagawa University, JAPAN*
[3] *Just corporation, Yokohama, Japan*
Email: shimazaki@kanagawa-u.ac.jp

ABSTRACT :

The recent aim of the earthquake resistant design is not only to protect life in very severe earthquakes, but also to use the buildings again after the earthquakes with small repair cost. A building system consisted with "coupled shear core walls with damper", CFT (Concrete Filled Steel Tube) columns, and flat plate slabs is one of the buildings having an ability of such demand. As floor load should be supported even in the large deformation at the CFT column-flat plate connection, it is required to avoid punching shear failure. To evaluate the vertical load resistance capacity of the newly designed CFT column-flat plate connection, experimental studies were carried out. The vertical force resisting mechanism of the joint zone is investigated and calculation can be made with fairly good accuracy by regarding a region with a shear force resisting vertical member as a truss system and regarding a region without such a member as an arch system. Vertical strength also can be calculated conservatively as a lower value of a simplified punching shear strength formula conforming to the ACI standard and a flexural yield strength value.

KEYWORDS: CFT Column, Flat plate slab, Joint, Vertical strength, Load resistance macro model

1. INTRODUCTION

As the performance requirements for building structures have diversified in recent years, demand for the protection of the property value of buildings from strong earthquakes is growing. In order to meet this demand, there is a need not only for the retention of structural performance but also for excellent repairability of structural members. The structural system shown in Figure 1, which is a structural system consisting of multilayer core walls connected by boundary beam dampers and concrete-filled-tube (CFT) column–flat plate (FP) frame system surrounding the core wall system, is one type of structure that meets such structural performance requirements. Compared with conventional reinforced concrete (RC) structures, the core wall and CFT–FP system has a number of advantages such as total weight reduction, longer spans, ease of construction and a high degree of freedom in space. The boundary beam dampers between the core walls absorb seismic energy, and the surrounding frame system mainly resists vertical forces. From the viewpoint of repairability after a severe earthquake, the behavior of the boundary beam dampers, which are short-span beams, is important. In this connection, we have already reported on boundary beams using debonded diagonal reinforcement [Shimazaki 2004]. Differences of a column–flat plate frame system, which mainly resists vertical forces, from a rigid-frame system include (1) two-dimensional stress distribution in the slabs, (2) stress redistribution occurring with the progress of concrete cracking and changing distribution patterns, (3) the coupling effect of horizontal forces and moments that makes the slabs prone to brittle punching shear failure. Regarding the horizontal force–deformation relationship at member joints, a method for setting restoring force characteristics has been proposed [Sato et al. 2004] with reference to past studies and the Standard for Structural Calculation of Reinforced Concrete Structures [AIJ 1998]. In this study, the vertical force resisting mechanism of the joint zone is investigated by conducted vertical loading tests on specimens modeling CFT column–flat plate joints including portions of slabs as shown in Figure 2.

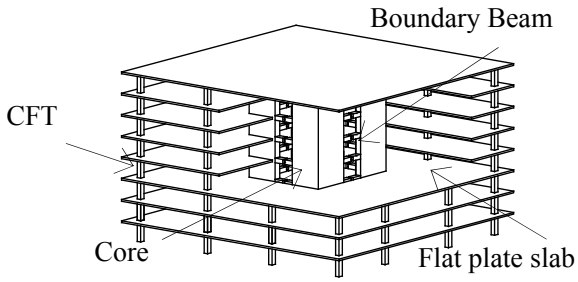

Figure 1 Prototype Building

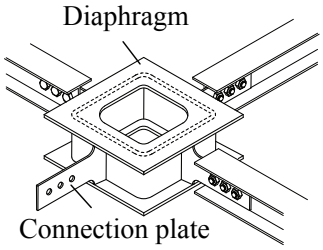

Figure 2 CFT column-flat plate connection

2. Experiment

In the loading tests, a structural element specimen modeling a CFT column–flat plate joint zone in a prototype building (Figure 1) was used. Each joint has a small embedded steel member. The stiffness and strength of this connecting zone are higher than those of other portions of the structural system, and the connecting zone behaves like a beam. Three series of tests were conducted, namely, Series I tests, in which reaction forces due to pushout loading are applied to the four sides of the specimen, Series II tests, in which reaction force is applied to four points at the four corners, two points or one point, and Series III tests, in which eccentric loads are applied to the joint zone and reaction force is applied as in the Series II tests.

2.1. Specimens

A total of 46 specimens were used; 13 specimens were used in the Series I tests, 27 specimens in the Series II tests, and 6 specimens in the Series III tests. Table 1 shows main parameters. All of the Series I and Series III specimens were cross joint specimens with a shear span ratio (M/Qd) of 1.3 (dimensions: 600×600×100 mm for Series II specimens and 660×660×100 mm for Series III specimens). For the

Table 1 Typical test specimens

Specimens of Ⅰ series				
Specimen	M/Qd	Connection plate h×b(mm)	Stud D(mm)	Slab reinforcing steel
Ps8	1.3	51×4	φ9	SD295
Specimens of Ⅱ series				
Ps14	1.3	51×4	D10	SD295
Ps16	2.0			
Ps20	3.4			
Ps21	1.3		φ6	USD785
Ps22				
Ps23			–	
Ps24		–	–	
Ps26		10×4	φ6	
Ps27		–	–	
Ps28		51×4	D6	
Specimens of Ⅲ series				
Specimen	M/Qd	Connection plate h×b(mm)	Stud D(mm)	Slab reinforcing steel	Eccentricity e(mm)
Es1	1.3	51×4	D6	USD785	0
Es2					100
Es3					200
Es4		10×4	–		
Es6		51×4	D6	SD295	

Table 2 Material properties

Specimen	Concrete	Compressive strength (N/mm²)	Tensile strength (N/mm²)	Young's modulus (N/mm²)
Ps8	Fc36	45.1	3.5	2.70×10^4
Ps21～27	Fc36	52.3	2.59	2.80×10^4
Ps28	Fc36	38.6	3.52	2.81×10^4
Es1～6	Fc36	39.5	3.37	2.86×10^4

Specimen	Steel materials		Yield strength (N/mm²)	Tensile strength (N/mm²)
Ps8	slab D6	SD295	463	567
	stud φ9	SR295	467	808
	PL-4	SS400	374	436
Ps14,16,20	D6	SD295	376	566
	stud D10	SD295	366	507
	PL-4	SS400	320	460
Ps21～27	D6	SD295	425	606
	U7.1	USD785	812	968
	stud φ6	SR295	554	754
	PL-4	SPHC270	251	357
Ps28,Es1～6	slab D6	SD295	385	552
	U7.1	USD785	782	949
	stud D6	SR295	363	505
	PL-4	SS400	251	357

Stud

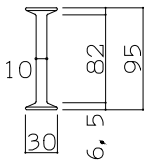

D10,φ9

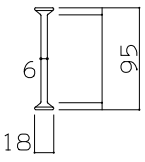

D6,φ6

Connection plate

51×4

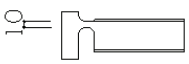

10×4（Ps26,Es4）

influence of cracking among the parameters for the Series I specimens, axisymmetric moment loading was carried out to introduce initial cracks so that steel strains around the joint zone at predetermined story drift angles became the values obtained in the previously reported frame tests. The Series II specimens consist of 14 cross joint specimens, one T-joint specimen, and six L-joint specimens. Three *M*/*Qd* ratios (1.3, 2.0 and 3.4) were set for the cross joint specimens, and their dimensions were 660×660×100, 820×820×100 and 1,100×1,100×100 mm, respectively. The *M*/*Qd* ratio for the T-joint and L-joint specimens was set at 1.3, and the dimensions of the T-joint and L-joint specimens were 660×460×100 and 460×460×100 mm, respectively. The Series III specimens were designed to investigate the influence of eccentric loading. Figure 3 shows representative specimens, and Table 2 shows summarizes the mechanical properties of the materials used.

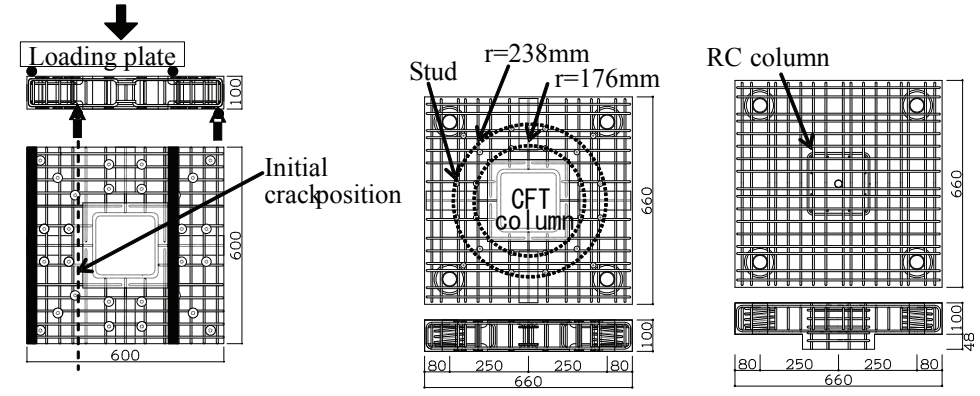

a) Ps8 and test setup of axisymmetric moment

b) Ps14

c) Ps27

Figure 3 Detail of specimens

2.2 Experiment method

Figure 4a) illustrates the loading methods used in the Series I, II and III experiments. In the Series I and II experiments, pushout loading was done by pushing the lower end of the CFT column of the structural element specimen with a 1,000 kN hydraulic jack. In the Series I experiments, reaction force was applied to the four sides of the specimen through reaction concrete blocks. As it turned out, the experiments practically became direct loading tests of the high-stiffness steel members. In the Series II experiments, reaction force was applied by pin loading through 100 mm diameter spherical supports. The T-joint and L-joint specimens had columns whose overall rotation was restricted. In the loading of the Series III specimens, eccentric force was given to the joint zone by installing an inverted-L-shaped steel member to the upper end of the CFT column of the structural element specimen and changing the loading location, and pushout loading was done by using a 1,000 kN testing machine.

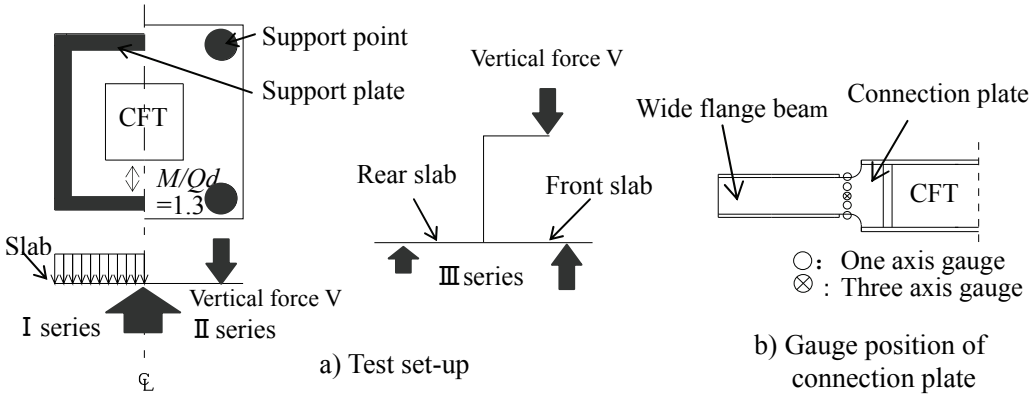

a) Test set-up

b) Gauge position of connection plate

Figure 4 Test set-up of CFT column-Flat plate joints

In the experiments, the vertical displacement of the diaphragm and the slab was measured. For the purpose of measurement, a single-axis strain gauge was attached to the upper and lower edges of the connection plate, a three-axis strain gauge was attached at the center of the web surface, and single-axis gauges were attached between those gauges (Figure 4b)). For the measurement of axial strain, single-axis gauges were attached to the slab. Vertical force was measured in terms of the sum of measurements obtained from the load cells installed to the prestressing tendons used for reaction force application (Series I and II) and was also measured with the 1,000 kN testing machine (Series III). The experiments were conducted by monitoring vertical force and the vertical displacement in the reaction zone to apply the load uniformly.

3. Experiment results

3.1 Load–displacement relationship

Figure 5a) shows the load–displacement relationships for representative Series I and Series II specimens. As shown, Ps8 and Ps21, which have normal-strength steel bars as slab reinforcement and are loaded differently, and Ps22, which has high-strength steel bars as slab reinforcement, show similar curves until 200 kN, after which Ps21 shows a decline in stiffness earlier than the other specimens and also shows differences in maximum strength. Ps26, which has a 10×4 mm connection plate, showed a slight decline in strength after the maximum strength was reached. Ps24, which does not have an embedded H-section or connection plate, and Ps27, which is an RC column, showed similar values of maximum strength, but Ps27 showed a sharp decrease in strength and failed in punching shear. Ps23, which has both an embedded H-section and a connection plate but does not have a stud, showed a similar value of maximum strength.

Figure 5b) shows the results for the eccentrically loaded Series III specimens. In the cases of Es1, Es2 and Es3, which are specimens that parameterize eccentricity (e), the maximum strength of Es2 (e = 100 mm) and Es3 (e = 200 mm) decreased to 76% and 52%, respectively, of Es1 (e = 0 mm). After the maximum strength was reached, all specimens excluding Es6 showed a decrease in strength.

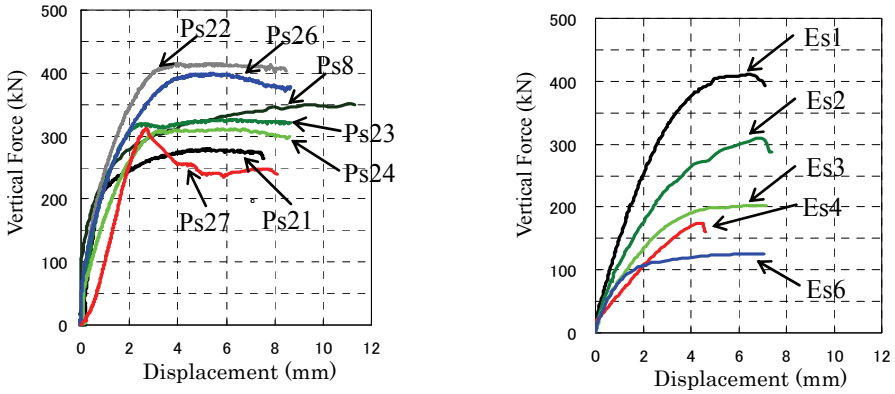

a)I,II series b) III series

Figure 5 Load-displacement relationship

3.2 Final state of cracking

Photo 1 shows the final states of cracking of the surfaces. In Ps8, which is a Series I specimen with an embedded H-section, cracks parallel with the H-section occurred first. After that, cracking occurred at 45 degrees from the column surface, and radial cracks resulted. On the upper surfaces of Ps14 to Ps21, which are Series II specimens that use normal-strength steel bars as slab reinforcement, cracks parallel with the embedded H-section occurred from the column surface, and on the lower surface of the slab, the region directly under the embedded H-section was crushed with the progress of deformation. In Ps22, which is a specimen that uses high-strength steel bars as slab reinforcement and has an embedded H-section, radial cracks occurred around the column as in Ps8, which is a Series I specimen. In Ps24, which is a specimen without an embedded H-section, cracks occurred at 45 degrees from the column surface, and the number of cracks parallel with the H-section was small. Ps27, which is an RC column specimen, showed a cracking pattern that is different from those of the other specimens; circular cracks occurred around the column and then the load decreased.

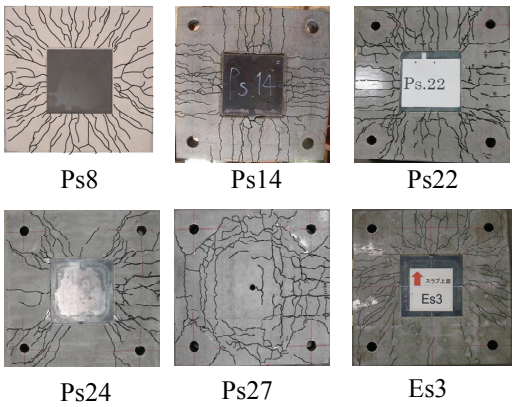

Photo 1 Crack pattern

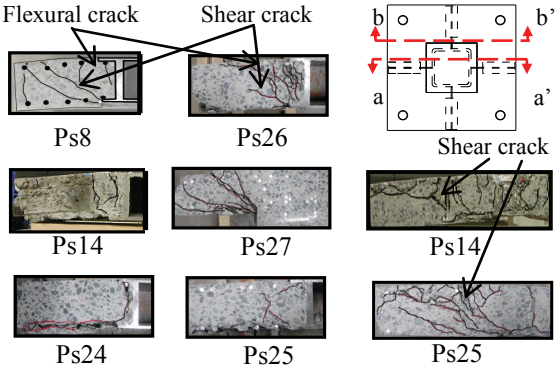

Photo 2 Internal crack pattern

Photo 2 shows internal crack patterns observed on cut surfaces of the specimens after the tests. The specimens were cut along section a–a', which is close to the joint zone, and b–b', which is close to the reaction force zone. In section a–a', Ps8, Ps26 and Ps27 showed clearly discernible shear cracks, while Ps14, Ps24 and Ps25 did not show such cracks. In section b–b', Ps14 and Ps25 showed clearly discernible shear cracks.

3.3 Reinforcement strain distribution

Figure 6a) shows the distribution of slab reinforcement strains at the maximum strength at locations A and A'. In Ps20, which is a specimen that uses normal-strength steel bars as slab reinforcement and has a high *M*/*Qd* ratio, strains at location A' located between the reaction support points were particularly large, and the slab reinforcement yielded in bending. In other specimens, too, strains at location A' were large. In Ps22 and Ps26 shown in figure 6b), which are specimens that use high-strength steel (USD785) bars as slab reinforcement, strains at location A' were large and a rising trend was shown in section A–A', but the strains were not so large as in Ps21, which is a specimen that uses normal-strength steel bars. In other specimens, strain distributions in section A–A' were roughly constant. The strain distribution in Ps27, which showed a sharp decrease in strength, showed lower values than other specimens. The strain distributions in the Series III specimens on the front zone of the slab were similar to those in the Series II specimens but showed relatively small values in the rear zone of the slab.

Figure 6c) shows stud strain distributions at locations (1) to (6). In all Series I, II and III specimens, stud strains at location (2) located at an angle of 45 degrees from the column surface showed relatively high values. In Es3, strains in the stud bars located at an angle of 45 degrees in the rear zone of the slab did not reach the yield level.

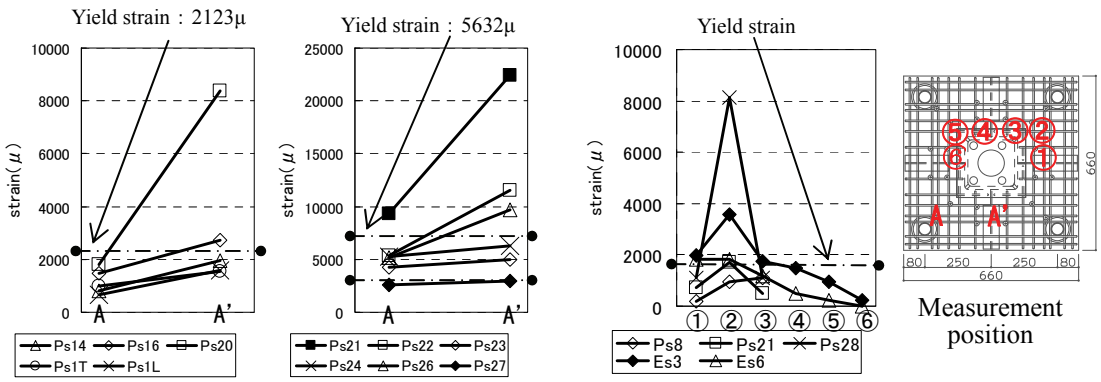

a) Normal-strength steel bars
b) High-strength steel bars
c) Stud strain distribution

Figure 6 Distribution of slab reinforcement strain

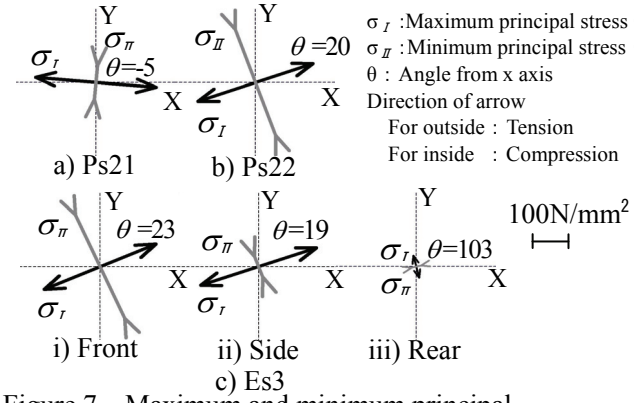

Figure 7 Maximum and minimum principal stresses in the connection plate

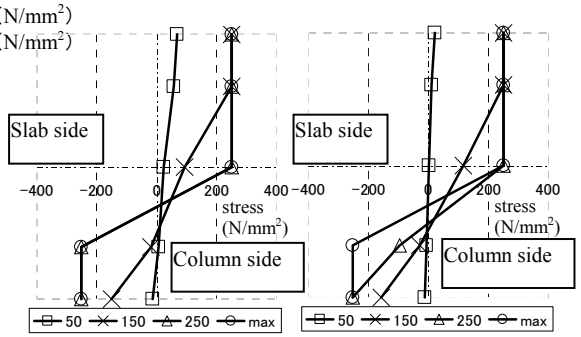

Figure 8 Connection plate stress distribution

3.4 Connection plate strain and estimated stress distribution

Figure 7 shows the maximum and minimum principal stresses in the connection plate before the maximum strength in Ps21 (flexural yield type specimen), Ps22 (shear failure type specimen) and Es3 (eccentrically loaded specimen) and the corresponding distribution angles. The maximum and minimum principal stresses were determined on the basis of material test results after calculating the maximum and minimum strains and their angles from the x-, y- and z-axis strains obtained from the three-axis gauges attached at the center of the connection plate. In Ps21, the angle to the maximum principal stress was close to 0 degrees, while in Ps22, it was about 20 degrees. It can be said that the connection plate of a shear type specimen resists shear stress while maintaining a certain angle until the maximum strength. In Es3, the angle of each connection plate was 23 degrees in the front zone, 103 degrees in the rear zone and 19 degrees in the size zone, indicating that the state of stress in the front zone of the slab is more critical than the states of stress in the other zones.

The connection plate stress distributions in Ps21 and Ps22 shown in Figure 8 show indicate that in both specimens, when the maximum strength was reached, the upper end yielded in tension and the lower end yielded in compression. On the whole, the region at depths of about 2/3 from the upper end resisted forces as a tension member, and the region at depths of about 1/3 from the lower end resisted forces as a compression member.

4. Evaluation of vertical strength of the joint zone

4.1 Flexural strength

The flexural strength V_m was examined, taking into consideration the final state of cracking and the strains in the slab reinforcing bars. Figure 9 shows the relationship between the calculated vertical strength V_m at the flexural yield strength and its measured values V_e for the flexural yield type specimens and the shear failure type specimens. For all flexural yield type specimens, measured values and calculated values show close agreement.

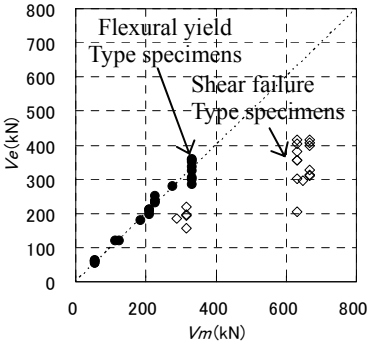

Figure 9 Flexural yield strength and measured values

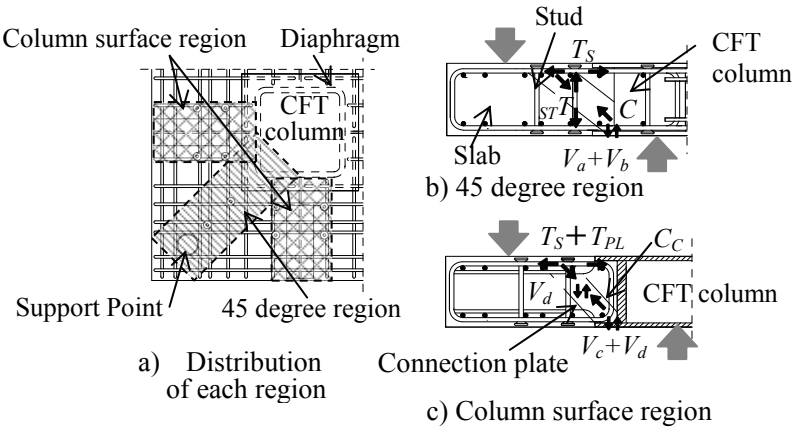

Figure 10 Resistance mechanism of the joint zone

4.2 Shear strength

In the case of the joint detail considered in this study, only the connection plate is connected to the CFT column. Consequently, the stress transfer mechanism in the joint zone becomes so complex that different load-carrying mechanisms occur in different regions. As shown in Figure 10a), the joint zone was largely divided into the 45-degree region (Figure 10b)) in which the slab load is directly transferred to the CFT, and the column surface region (Figure 10c)) in which the load transferred to the H-section is transferred indirectly. These regions were further subdivided into regions with shear resistance members and regions without shear resistance members. It was assumed that in each region, an arch mechanism is formed when the slab reinforcement (T_S) and the connection plate (T_{PL}) function as horizontal tension members and the concrete performs the function of compression struts (C_C). It was also assumed that if there is a stud bar ($_{ST}T$), which is a vertical tension member, or an H-section or a connection plate ($_{PL}T$) that provides reaction force to the concrete strut in that region, then a truss mechanism is formed. If the slab reinforcing bars were anchored in the concrete strut with 180-degree hooks as shown in Figure 10c), the slab reinforcing bars were regarded as horizontal tension members.

Vertical strength was calculated by this model with calculating the strength of the horizontal tension members from the measured strains at the maximum strength of the slab reinforcement and the connection plates of the shear failure type specimens and from material test results. For the eccentrically loaded specimens, strength was calculated in the region in front of the column and the 45-degree region, taking into consideration the torsional resistance of the side zones of the slab. Figure 11 shows the relationship between the calculated values and the measured values. Since the measure value/calculated value ratio shows values close to 1 (one), the shear strength of the joint zone can be calculated by using these models. Even under the influence of these shear forces, stresses can be transferred to the CFT by the shear strength of the diaphragm cross section.

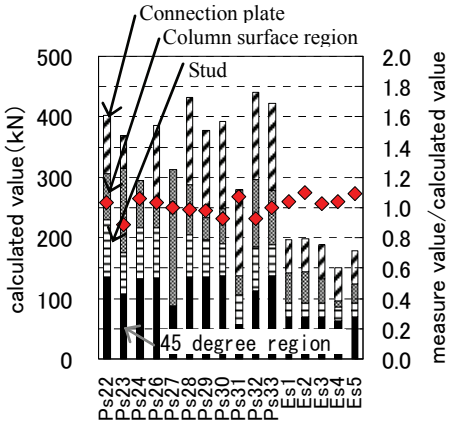

Figure 11 Calculated value and measure value

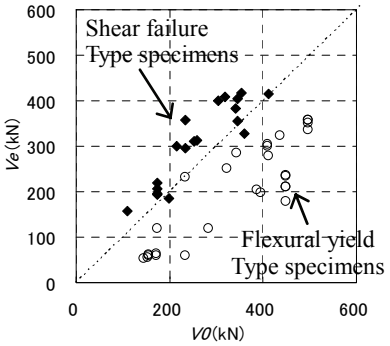

Figure 12 Punching shear strength and measured values

5. Adaptability of conventional shear strength formula

The calculation method using the load-carrying mechanism models is unwieldy to use. In this section, therefore, conformity with the ACI standard (ACI 421.1R-99) is evaluated. The ACI standard calculates shear strength as the sum of the allowable shear force for concrete and the allowable shear force for studs, so Eq. (5.1) was derived by adding the allowable shear force for the connection plate to the above.

$$V_0 = {}_sV + {}_{st}V + {}_cV \quad \text{---------- (5.1)}$$

where

$_sV$: allowable shear force for connection plate

$$ {}_sV = {}_{pl}n \frac{{}_{pl}f_t}{\sqrt{3}} A_{pl} $$

$_cV$: allowable shear force for concrete

$$ {}_cV = {}_c\alpha \sqrt{{}_cf_c} A_c $$

$_{st}V$: allowable shear force for stud

$$_{st}V = {}_{st}n \cdot {}_{st}a_t \cdot {}_{st}f_t$$

$$A_c = 2d_s(c_1 + c_2 + 2d_s)$$

$_c\alpha$ = 0.33 (concrete cross section only)

$_c\alpha$ = 0.165 (stud taken into account)

$_{pl}f_t$: allowable tensile stress for connection plate

A_{pl}: cross-sectional area of connection plate

$_{st}f_t$: allowable tensile stress for stud

d_s: effective depth of slab

$_cf_c$: allowable compressive stress for concrete

A_c: area of critical cross section

$_{st}a_t$: cross-sectional area of stud shaft

$_c\alpha$: coefficient for shear stress resisted by concrete

$_{pl}n$: number of connection plates in the cross section of interest

$_{st}n$: number of studs in the cross section of interest

c_1: width of column surface in the direction perpendicular to horizontal force

c_2: width of column surface in the horizontal direction

Figure 12 shows the relationship between the measured value V_e for each specimen and the punching shear strength V_0 calculated from Eq. (5.1) on the basis of material test results. For the purpose of calculation, the specimen was divided into regions as shown in Figure 10, and the ratio of shear force resisted by each specimen was taken into consideration. The studs to be taken into account were the first-row studs located in the 45-degree direction from the column surface. The V_e/V_0 ratios for Ps13, Ps24, Ps26 and Ps27, which showed shear failure behavior, were 1.0 or greater, indicating that they were on the safe side. As shown in the shear resistance mechanism model, the effect of the concrete compression strut in the joint detail is thought to be great. Eq. (5.1) may be used as an approximation formula for punching shear strength.

6. Conclusion

This study investigated the vertical load carrying mechanism of the proposed CFT column–flat plate connection and evaluated a strength formula. The findings of this study can be summarized as follows:

1. The connection plate and studs contribute to shear strength, and the studs perform the function of vertical tension members as a truss system.
2. For shear resistance mechanism modeling, the joint zone was divided into a 45-degree direction region and a column surface direction region. These regions were further divided into regions with shear resisting vertical members and regions without them. Calculation can be made with fairly good accuracy by regarding a region with a shear force resisting vertical member as a truss system and regarding a region without such a member as an arch system.
3. Vertical strength can be calculated conservatively as a lower value of a punching shear strength formula (Eq. (1)) conforming to the ACI standard and a flexural yield strength value.

ACKNOWLEDGMENT

This study was funded by Grants-in-Aid for Scientific Research of JSPS. The opinions and findings do not necessarily represent those of the sponsor.

REFERENCES

Shimazaki, K. (2004). De-bonded diagonally reinforced beam for good repairability, *13th World Conference on Earthquake Engineering*, **Paper 3173.**

Satoh, H. and Shimazaki, K. (2004). Experimental research on load resistance performance of CFT column/flat plate connection, *13th World Conference on Earthquake Engineering*, **Paper 976**.

Architectural Institute of Japan (1999) AIJ Standard for Structural Calculation of Reinforced Concrete Structures －Based on Allowable Stress Concept－

ACI-ASCE Committee 421, Shear Reinforcement for Slabs、ACI 421.1R-99